SEMIANNUAL STATUS REPORT

FOR PERIOD 1 JULY 1966 THROUGH 31 DECEMBER 1966

Required under the terms of NASA Research Grant NsG 443 - 29

"Research Related to an Experimental Test of General Relativity"

Under the Direction of

H. W. Knoebel and W. D. Compton

COORDINATED SCIENCE LABORATORY
University of Illinois
Urbana, Illinois

March 1967

1. Introduction

A passive non-metallic gyroscopic earth satellite for measuring the in-plane precession predicted by general relativity is being studied. Gravity gradient torques are minimized by the combination of optimum gyroscope geometry and favorable initial alignment of the spin axis. Data are recovered by observation of flashes of solar reflection from mirrored facets on the satellite.

2. Optimization of Parameters

Selection of optimum orbit and satellite size and shape parameters for a relativity experiment is being studied. The objective is to select parameters in such a way that the expected relativity effect is maximized while disturbance torques are minimized and to provide for a sighting frequency high enough to yield accurate measurement of the spin axis orientation for an extended period of time, of at least one year. A summary of the principal factors in orbit selection follows, assuming the orbit is circular.

(1) The effect to be measured – predicted by the general theory of relativity – is maximized when the satellite spin axis is in the plane of the orbit and varies inversely as the orbital radius raised to the 5/2 power.[1] Either a non-regressing polar orbit or an equatorial orbit would permit the gyro spin axis to remain in the orbital plane for an extended period of time.

(2) Disturbance torques produced by gravity gradient and by aerodynamic drag are both minimized when the spin axis is in the orbital plane, but the latter is two orders of magnitude smaller at an altitude of 1000 km. These effects are documented in CSL reports.[1,2,3,4] Minimization of these torques for an extended period also implies that either a polar or an equatorial orbit must be used.

(3) Solar pressure torques may be the most serious disturbances from the standpoint of uncertainties.[1] That is, the amount of torque may change during a year's time because of degradation of the satellite surface and resulting imbalances of absorptivities between the two

satellite hemispheres. Therefore, the proposal of a polar orbit with the gyro spin axis normal to the ecliptic plane is not ideal because precessions due to solar pressure torques of unknown changing magnitude could easily exist in the plane of the orbit and invalidate any suspected measurement of the relativity effect. This uncertainty would exist in any polar orbit, regardless of the spin axis orientation. The use of an equatorial orbit would allow the spin axis to lie in both the orbital and ecliptic planes and solar pressure torque would cause precessions with out-of-plane components predominating, and therefore would not be confused with in-plane measurements. In this configuration the uneven heating of the satellite may produce unsymmetrical thermal expansion and result in slight variations in the directions of mirror normal angles. The amount of the variations will depend on the slowly changing angle between the satellite spin axis and the sun line, but can be corrected for in the data reduction or minimized by using a "zero expansion" material such as Owens-Illinois "Cer-Vit".

(4) Reduction of electromagnetic torques was the primary consideration in proposing a passive satellite, and material properties have been specified such that precessions due to these torques will be at least one order of magnitude lower than the relativity effect regardless of the orbital parameters.[2] Material properties and shape parameters are also the most important factors in reducing disturbances due to micrometeoroids.[2,5]

From these considerations the equatorial orbit seems the logical choice. The frequencies of sighting a satellite in an equatorial

orbit from certain tracking stations are being determined by a digital computer simulation. Results of computations for a 1000 km orbital altitude indicate a possibility of sighting the satellite about twice a day, weather permitting, from each of two Baker-Nunn tracking stations located at Curacao (n. latitude = 12^{o}) and Arequipa, Peru (s. latitude = 16.5^{o}) and operated by the Smithsonian Astrophysical Observatory.[5] Other stations in the SAO network could not be used for tracking the orbit specified above chiefly because of a lower limit of 15 degrees on the elevation of the Baker-Nunn cameras. Besides the elevation limit, two other criteria for sighting the satellite are employed in the digital simulation: (1) at the station in question, the observing time must be at least 2/3 hour before sunrise or 2/3 hour after sunset; (2) the satellite must be in sunlight. During each simulated pass, the angle from the satellite spin axis to the hypothetical mirror normal which would reflect sunlight to the observing station is computed by a technique described by Hill.[6] In general, the distribution of these flash angles is different for each pass. Figure 1 shows a typical flash angle distribution for an observing station at Curacao. The data shown in this plot were computed using the criteria cited above and with the satellite spin axis directed along the vernal equinox. These data indicate that a satellite with mirrors located at say 40, 80, and 140 degrees could be sighted continuously for one year from this station, weather permitting. An additional sighting criterion, based on the light threshold at the Baker-Nunn camera,[5] will depend on the slant range and the projected cross-sectional area of the reflecting mirror at the time of

Station latitude = 12.^{o} Orbit inclination = 0.0^{o}

Station East longitude = 291.^{o} Eccentricity = 0.0

Satellite altitude = 1000.km

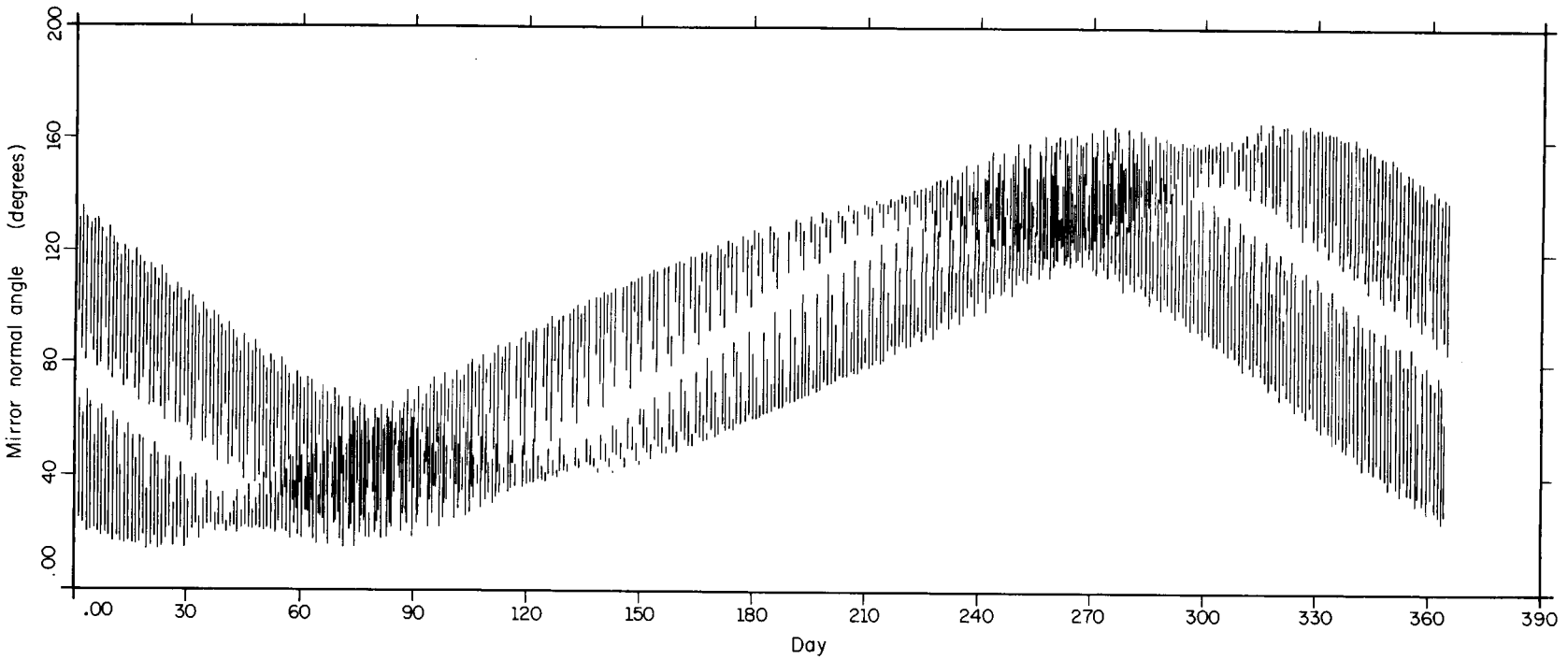

Fig. 1. Flash angle distribution for tracking station at Curacao. Satellite spin axis aligned along the vernal equinox line.

observation. This additional criterion will either reduce the expected sighting frequency for the proposed 30 cm diameter satellite, or necessitate a revision of the satellite size and mirror areas.

To increase sighting frequency for the 1000 km orbital altitude, low inclination orbits will be simulated, so that some observations can be made from other stations in the SAO network. Inclinations up to 10^{o} may be feasible without excessive attitude drift rates from extraneous sources. The largest of these, the gravity gradient precession for a low inclination orbit, is given by[3]

$$\Delta\varphi \approx \Lambda[\delta_e \, t + \frac{i}{\dot{\Omega}} (1 - \cos \dot{\Omega} \, t)],$$

where $\Delta\varphi$ is the component of gravity gradient precession in the earth's equatorial plane in time t, Λ is the gravity gradient precession coefficient, δ_e is a small angle between the satellite spin axis and the earth's equatorial plane, i is the orbital inclination, and $\dot{\Omega}$ is the nodal regression rate of the orbit. Minimization of Λ with respect to gyro diameter[2] gives a typical value of 80 sec arc per year. For a 10 degree inclination, the nodal regression rate is 2200 degrees per year, and the maximum excursion in the periodic component of $\Delta\varphi$ is less than one second of arc. The secular component of $\Delta\varphi$ depends only on δ_e and is independent of i. At 10 degrees inclination the satellite could be tracked for limited times by three additional stations in the SAO network, at latitudes of 21^{o}, -26^{o}, and 27^{o}.

3. Solar Radiation Pressure Torque

In the Semiannual Status Report for the period of 1 January 1965 through 30 June 1965, an approximation was made of the precession of a spinning satellite under the action of solar-radiation-pressure-induced torque. Since the estimation was made using rather uncertain parameters a more complete investigation was initiated on this problem during this period.

Many authors have treated the problem of solar radiation pressure torque where the radiation disturbance torque arises from the asymmetry of the surface presented to the radiation source or from shielding of surfaces from radiation (see for example ref. 7). For the C.S.L. satellite, shielding effects are non-existent and torques arising from asymmetry of the surface will be extremely small due to the nearly spherically symmetric configuration of the satellite. However, even when the surface is symmetrical with respect to the center of mass, a torque can exist because of differential reflectivity of surface elements and variations in the direction of the surface normal. Different values of reflectivity for the various surfaces could arise from differential exposure to solar radiation, meteorite cratering, manufacturing errors and other causes. Variations in the direction of the surface normal could arise from manufacturing errors and warpage of the surface due to deformation under centrifugal stress while spinning and thermal expansion caused by solar heating. A statistical approach such as that presented by Robert E. Roberson[8] will be applied to the C.S.L. satellite to include those effects mentioned above. This approach will then

give an expected value of precession due to the combination of these effects. This entire analysis has not yet been completed but some important preliminary results have been obtained which can be reported at this time.

First, a computer program has been written for use on C.S.L.'s Control Data 1604 computer to calculate the precession caused by differential reflectivity of the various surfaces on a C.S.L. satellite. The program itself is general enough to be useful for calculating solar radiation induced precession of spinning satellites of many different configurations. The orbit must be circular but may have any inclination and altitude. The orbital regression and earth shadow effects are included in the calculation.

For purposes of numerical computation, the satellite parameters used in the first calculation were for the satellite configuration reported in the Semiannual Status Report for the period 1 January 1966 through 30 June 1966. Briefly, the configuration is a sphere modified by cubic-oriented flat surfaces. The spherical diameter is 30 cm and the flat to flat diametric distance is 24.50 cm. The six surfaces each have area of 236 cm^2 and the angles of the surface normals relative to the spin axis are 42, 54, 71.36, 108.65, 126, and 138 degrees. An equatorial orbit of 600 miles, or approximately 1000 km, altitude was chosen with the spin axis in the plane of the orbit and initially perpendicular to the earth sun line and the vernal equinox line.

Differential reflectivity was introduced into the problem by considering each surface to independently have a coefficient of

reflectivity, η, of zero while the other five surfaces were treated as being perfect mirrors, $\eta = 1$. In this manner, many different combinations of differential reflectivity were generated. The results of the calculation show that the "out of plane" precession, $\dot{\theta}_s$, is periodic returning to zero in one year and with a maximum absolute value of total angular change of

$$|\Delta\theta_{s_{max}}| = 1.19(1-\eta) \text{ sec of arc.}$$

The "in the plane of orbit" precession, $\dot{\phi}_s$, is found to have both secular and periodic components. The maximum absolute value of total angular change in one year's time of this precession occurs near the end of the year and was found to be

$$|\Delta\phi_{s_{max}}| = 1.12(1-\eta) \text{ sec of arc.}$$

This value is the largest such precession that will occur for an equatorial orbit with the spin axis in the orbital plane. For the special case when the satellite spin axis lies in both the equatorial orbital plane and the ecliptic plane, the "in the plane of the orbit" precession is periodic returning to zero in one year and having a maximum angular change of

$$|\Delta\phi_{s_{max}}| = 0.62(1-\eta) \text{ sec of arc.}$$

From these preliminary results, we can see that even for a 10% decrease in reflectivity of a mirror surface, the maximum amount of precession would be about one-tenth of a sec of arc which would not interfere with a measurement of the relativity effect.

Now, consider a small area having zero reflectivity such as could take place if a meteorite impacted at a point on the spherical part of the satellite. We can apply the results we have to this problem also. Consider the area to be one-hundredth the area of a mirror flat. Since the solar radiation pressure torque, and therefore the precession, is directly proportional to the area of the surface in question we can, as an approximation, assume that the maximum precession in one year is 1/100 of that we have calculated; i.e.,

$$|\Delta\theta_{s_{max}}| \simeq |\Delta\phi_{s_{max}}| \approx 0.01 \text{ sec of arc.}$$

Precessions of this magnitude can be neglected.

We see, therefore, that the solar radiation pressure torque is an important disturbing torque, but, on the basis of these preliminary results, the effect of this torque is reduced significantly if the reflectivity of the surfaces is balanced to within 10% of each other.

4. Gyro Materials

A more exact analysis of the passive damping method for aligning the instantaneous spin, symmetry and angular momentum axes of the gyro satellite has been completed and reported.[9] Damping is accomplished by the dissipation of energy due to cyclic strains in the gyro caused by its torque-free precession. The gyro was considered an axially symmetric solid, spherical in shape except for two diametrically opposite flats which give a preferred moment-of-inertia C. The moment-of-inertia about a perpendicular axis is A.

In the previous report an approximate value of the total gyro elastic strain energy W was calculated, from which the hysteretic damping factor γ was calculated for a given damping time t. The exact analysis of W shows that it can be classified into two parts. The first is a very slowly varying quantity which, for practical purposes, can be considered a steady or dc part. The second part varies with time at a fundamental rate $\dot{\phi}$ (referred to as the elastic vibrating frequency) and all higher harmonics of $\dot{\phi}$ up to the fourth. The quantity $\dot{\phi}$ is the angular rate at which the instantaneous spin axis moves about the gyro body as viewed by an observer stationed on the body. It is this time varying part which is responsible for the hysteretic damping of precession.

Reference 9 shows that W is a function of gyro radius a, gyro material, spin speed ω_o and angle θ (misalignment between the gyro angular momentum axis and symmetry axis) as in the following equation for small values of θ:

$$W = \frac{4\pi^2 \rho \omega_o^4 a^7 \theta^2 \Gamma}{E} \tag{1}$$

where ρ is the density, E is Young's modulus and Γ is a dimensionless quantity which is a function of gyro geometry and material. When this is substituted into the equation for damping time t as given in the previous report, with $\sin \theta \approx \theta$, the equation for damping time becomes

$$t = \frac{4E}{15\gamma\, \omega_o\, \Gamma\, \rho \omega_o^2\, a^2} \ln \frac{\theta_f}{\theta_i} \tag{2}$$

where θ_i and θ_f are the initial and final misalignment angles, respectively, and γ is the hysteretic damping factor.

From elasticity theory,[10] the maximum stress at the center of the solid, spinning sphere is approximately given by

$$\sigma_{max} = \rho\omega_o^2 a^2 \left(\frac{3 + 2\nu}{7 + 5\nu}\right) \tag{3}$$

where ν is Poisson's ratio. Hence, the term $\rho\omega_o^2 a^2$ in the denominator of Eq. (2) is proportional to the maximum allowable stress for the selected gyro material. The analysis of the combined effects of gravity gradient, centrifugal distortion and the statistics of micrometeorite cratering leads to an optimum gyro diameter of about one foot.[2] Equation (3) therefore establishes the maximum ω_o for a given gyro material giving due allowance for a safety factor. For plate glass, for example, the tests described in the previous report indicated an upper value of ω_o of about 630 rad/sec, with an adequate safety factor. For this same material and for the following parameters:

$$\gamma = \frac{2\pi}{Q} = .025$$

$$\rho = 2.5 \times 10^3 \text{ kgm/m}^2$$

$$\omega_o = 630 \text{ rad/sec}$$

$$a = 7.5 \text{ cm} - .075 \text{ m}$$

$$\theta_f = 0.1 \text{ arc sec}$$

$$\theta_i = 30 \text{ arc min}$$

$$E = 7 \times 10^{10} \text{ Newtons/m}^2$$

$$\nu = 0.16$$

the value of Γ, from reference 9, becomes .071, which, when substituted into Eq. (2) gives a damping time of 8.2 hours.

For a gyro of one foot diameter the analysis of micrometeorite cratering[11] gives a relationship between the number of hits per year, each of which could cause an angular disturbance of 0.6 arc sec per year, versus (C-A)/C. For one hit per year the ratio $(C-A)/C \approx 0.01$. Assuming a Poisson distribution for the meteorite flux, this gives a probability of 0.92 for having one month of undisturbed data. It is important, then, that the damping time be quite smaller than one month in order to separate the effects of such cratering from the spin axis orientation data. The above analysis shows that this condition is satisfied.

In conclusion, therefore, using glass as a possible gyro material, the passive damping method for aligning the gyro instantaneous spin axis, angular momentum axis and symmetry axis has been shown to be feasible, requiring about 8¼ hours to damp from θ = 30 arc min to θ = 0.1 arc sec. The damping time constant τ is 0.83 hours, which is probably required only during the initial gyro spin-up. The effect of a micrometeorite collision which would cause an angular disturbance of 0.6 arc sec per year would require only 1.5 hours to damp to 0.1 arc sec, a reasonable time.

5. Spin-Axis Readout Studies

Investigations of the accuracy with which the spin-axis-orientation data may be obtained for the relativity satellite experiment have continued during this reporting period. As explained previously,[12] the investigations focus upon the accuracy with which the positions of long streak-like images, exhibiting a symmetrically tapered density, may be determined on the photographs produced by the Baker-Nunn cameras operated by the Smithsonian Astrophysical Observatory. The nominal accuracy of $\pm$ 1.1 seconds of arc, obtainable for "hard-edged" images, would more than suffice for the purposes of the proposed experiment. The goal of the present investigations is to make a quantitative determination of the degree to which that accuracy is approachable by the "soft-edged" images to be dealt with in the proposed experiment.

Put another way, the goal is to determine the exposure level (which determines the signal-to-noise ratio, for the image being the signal, and the photographic-film grain being the noise) necessary to attain particular levels of accuracy. These exposure levels are to be compared with the nominal camera input of 8×10^{-11} lumen-sec/m^2 producing a density of 0.3 to 0.4 units above night-sky background, an exposure level found consistent with the proposed satellite parameters. In this way, quantitative determinations of the "pay-off" inherent in adjustment of these parameters may be made.

The investigations are proceeding by two routes of simulation, a "theoretical" one in which the simulation of center-estimation procedures of simulated noisy images is conducted in the CDC-1604 computer,

and an experimental one in which the corresponding images are produced on film by optical means for evaluation by optical methods. Aspects of the computer methods are described in sections 6 and 7 below, together with section 8 which describes the procedures being followed to obtain the necessary empirical data for use in the computer simulation. Section 9 describes the procedures to be followed in the experimental approach.

6. Calculation of Simulated Film Noise

The probability distributions for the grain noise of photographic film qualitatively resemble Gaussian distributions except for being somewhat skewed. It is clear that perfectly symmetrical distributions are out of the question whether for transmission values, $t = I/I_o$, the ratio of transmitted to incident light intensity, for opacity values, $\omega = 1/t$, or density values, $\delta = \log\omega$. For transmission values bounded to the finite interval $0 \leq t \leq 1$, the distribution must vanish at 0 and 1 and be appropriately skewed as the mean "crowds" close to either bound. Opacity values are bounded to the semi-infinite interval $1 \leq \omega < \infty$, and density values are bounded to a similar interval $0 \leq \delta < \infty$. For the latter two, a noise-distribution model that is skewed for mean values near only one finite bound, and which tends to a gaussian form as the mean value moves far from the bound, is needed.

The notions of "nearness" and "farness" of the mean from the bound is measured relative to the standard deviation, so that the simplest mathematical form that would satisfy these needs would, in addition to scaling and shifting parameters, require one more parameter,

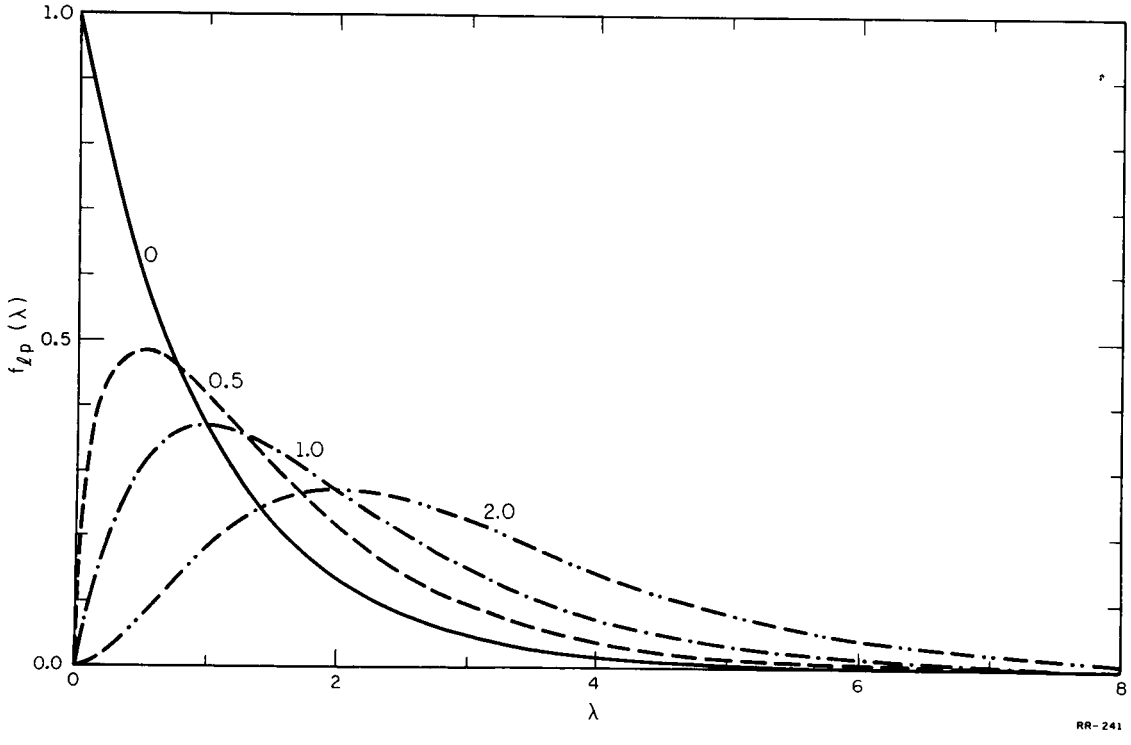

Fig. 2. Plots of probability density functions to be used in simulation of film noise. The parameter p is related to the ratio of mean to standard deviation.

the ratio of mean to standard deviation. Such a distribution is the chi-squared distribution having the differential form

$$f_{\ell p}(\lambda)d\lambda = [\Gamma(p+1)]^{-1}e^{-\lambda}\lambda^{p}d\lambda, \tag{4}$$

governing a random variable $0 \leq \ell_p < \infty$, with mean value $\nu_{\ell p} = p+1$ and standard deviation $\sigma_{\ell p} = \sqrt{(p+1)}$. Given arbitrary values of mean and standard deviation, ν_x and σ_x, then the random variable ℓ_p with p set equal to $(\nu_x/\sigma_x)^2-1$, may be used to form the random variable x via

$$x = \sigma_x^{\,2}\ell_p/\nu_x. \tag{5}$$

Also, for large values of the ratio ν_x/σ_x, that is to say large values of p, this distribution approaches a gaussian form. Plots of $f_{\ell p}(\lambda)$ are shown in Fig. 2 for p = 0, 0.5, 1, and 2.

For computer-simulation purposes, the random variable ℓ_p is formed from uniformly-distributed ones u, v in various ways, depending upon the value of p. For example, when p = 0 the distribution (4) is just the exponential distribution which in cumulative form is

$$F_{\ell 0}(\lambda) = \int_0^{\lambda} e^{-t}dt = 1-e^{-\lambda}, \tag{6}$$

with inverse

$$\lambda = F_{\ell 0}^{-1}(F) = -\ln(1-F), \tag{7}$$

from which formula ℓ_0 is formed from the uniformly distributed variable $0 \leq u < 1$ as $\ell_0 = F_{\ell 0}^{-1}(u)$.

When p is not an integer, the inversion of the cumulative version of Eq. (4) is very time consuming, as are the calculations of the gamma (factorial) function. In such a case, $0 < p < 1$, the independent random variables u,v are regarded as determining a point in the u,v plane, in which is also plotted the curve

$$v = e^{-u} u^{p}, \qquad 0 < p < 1. \tag{8}$$

The computer then tests v to see if it lies below the curve. If so, then the random variable ℓ_p is taken equal to these selected instances of u. If the test fails, the roles of u,v are interchanged, and the test is repeated. If it fails again, both instances of u,v are discarded, and a new pair is generated, continuing until a success is found. The variables u,v are scaled for this test so that a suitably large fraction of the area under the curve, e.g., 99.9%, is covered.

When the value of p is not less than unity, it is analyzed into a fractional part, $0 \leq p_f < 1$, and an integer part, $p_i = n$. Then, advantage is taken of the fact that

$$\ell_p + \ell_0 = \ell_{p+1} \tag{9}$$

for ℓ_p and ℓ_0 independent. Thus, n independent generations of ℓ_0 are summed together along with one generation of ℓ_p for $p = p_f$.

For p = 10 or larger, the computation becomes excessively long by the above methods. Also, the ratio of mean to standard deviation is larger than 3.3. For such cases, the gaussian approximation is justified. A gaussian variable is calculated <u>via</u> stored-table lookup, using

$$\ell_p\text{-}(p+1) = \sqrt{(p+1)}F_g^{-1}(u) \ ,$$

in which F_g^{-1} is the inverse of the cumulative gaussian distribution for zero mean and unit standard deviation.

7. Simulation of Center Estimation

The film-noise model is used to generate a simulated image as a sequence of measurements along the long axis of the narrow image. The noise model described above may be used to simulate either a density sequence or an opacity sequence. Laboratory measurements that used an optical weighting of the image (with density wedges, for example) would be weighting opacity values, however. In the computer, the mean value of noise at a given point along the image is made to conform to the mean value produced by the photographic exposure at that point, using the relation between opacity (or density) and exposure given empirically by the H & D curve for the photographic material intended for use. Similarly, the noise variance at such a point is to be related to the mean value by an empirical relation appropriate to the optical resolution hypothesized for the formation of the image. Determination of this second empirical relation is described in section 8 below.

Pending the availability of the noise-variance data, the computer program has been exercised using an arbitrary choice for that variance. Figure 3 shows a plot of such a noisy-signal sequence. The choice made was that of a constant variance with a distribution bounded to $0 \leq \delta < \infty$. As it happens, the bound-and-variance choice for this exercise agree with the subsequently-obtained data describing density.

Very similarly-appearing plots would be generated for opacity bounded to $1 \leq \omega < \infty$, except that the standard-deviation of the noise would increase approximately linearly with increasing mean opacity.

In the plot, the abscissa simulates the position along the image and the ordinates the noisy signal values. At the left and right are statistically stationary intervals corresponding to no-signal background. As the sequence enters the image from the left, say, the mean value is caused to increase and follow an elliptical curve (the H & D distortion was not inserted in this exercise) with a peak mean-to-standard-deviation ratio (SNR) of 10. The image is 180 resolution units wide, corresponding to a width of 1800 seconds of arc with a resolution of 10 seconds.

For center estimation, a fixed weighting pattern was used that assigned zero weight outside an interval corresponding to the width of the expected image and a linear (or center-of-gravity-estimating) weight within the interval. A plot of this weighting function would resemble the letter N. The noisy-image signal values are then multiplied by the weight values, for the center of the weighting pattern being located at an arbitrary point relative to the center of the image, and the weighted values are summed. The computer repeats this procedure for a sequence of locations for the center of the weighting pattern until it finds a location for which the sum is null. This null location, which is almost always unique even for much noiser images than shown, is the estimate of the center.

The center estimate for the image shown deviates from the true center by 0.16% , or -0.30 resolution units corresponding to -3.0

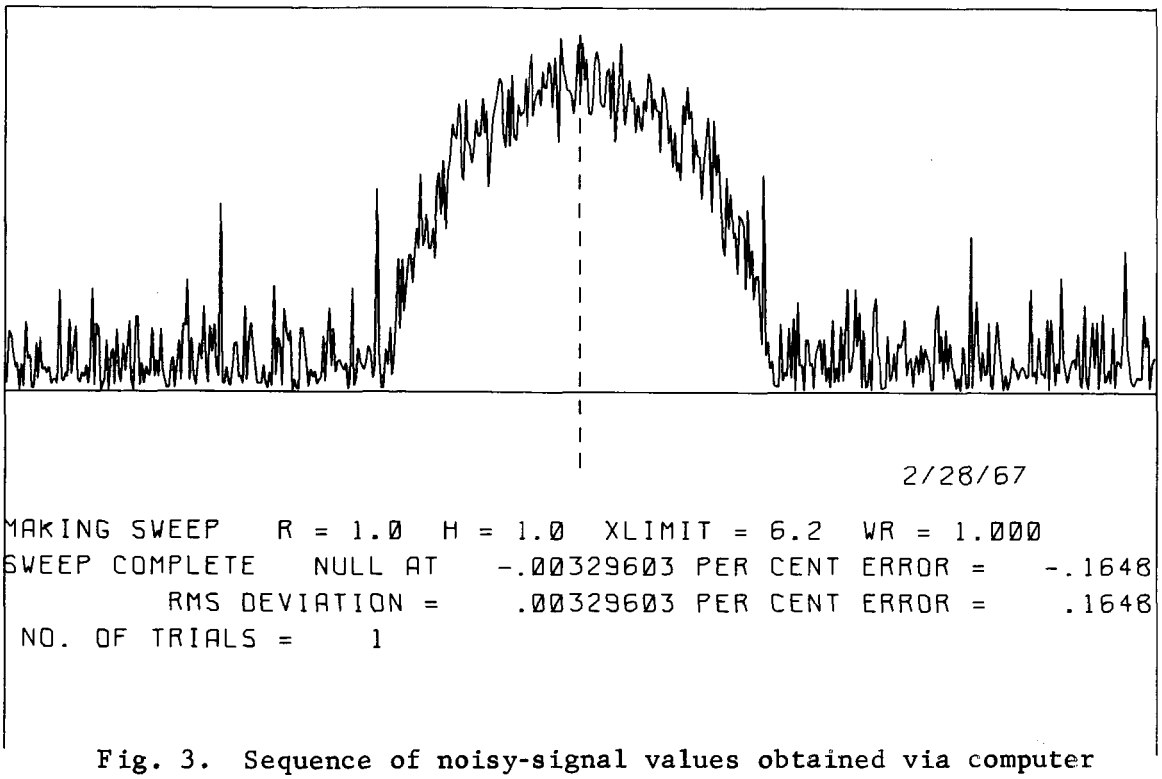

Fig. 3. Sequence of noisy-signal values obtained via computer simulation. The standard deviation was held constant while the means traced out an elliptical signal pattern. Fifty such trials were made with an rms center-estimation error of 0.29%.

seconds of arc. This exercise has been repeated for 50 statistically-independent images with estimates that turn out to be symmetrically distributed about the true center and to have a standard deviation of 0.2862%, or 0.51 resolution elements, corresponding to 5.1 seconds of arc. For this exercise model and choice of peak SNR, this would constitute the accuracy appraisal.

In the next few months, more realistic simulations will be performed, providing an accuracy appraisal as a function of peak exposure for the relativity experiment. Such an appraisal will result in a determination of the peak photographic exposure needed, at minimum, to fulfill minimal accuracy requirements for the experiment.

8. Measurements of Photographic Film Noise

The measurement of film noise is based on projection-microphotometer tracings of step wedges recorded on Royal-X Red-Extended photographic film. These step-wedge specimens were supplied by the Smithsonian Astrophysical Observatory. The raw data consist of transmission values obtained on a specular basis (scattered light from the film specimen does not significantly contribute to the transmission) and recorded *via* an analog-to-digital converter on punched paper tape. The resolution used was 20 microns corresponding to about 10 seconds of arc.* Readings at

*Actually nearer 8 seconds of arc. The spatial power bandwidth is proportional to the reciprocal of the area of the resolution window, however, so that the standard deviation for neighboring resolutions will be proportional to the reciprocal of the resolution.

least one resolution-interval apart along the film were taken to guarantee statistical independence among the readings. A typical tracing, replotted via CALCOMP from the papertape record is shown in Fig. 4. Relatively short runs were made so that accurate focus could be guaranteed as necessary to assure constancy of the resolution interval and hence statistical stationarity.

Calibration of these tracings was undertaken via reference to similar tracings made from a calibrated Welch density step wedge. The Welch calibration is based, however, on diffuse transmission measurements (almost all the forward-scattered light contributes to the transmission). Using the rule that the diffuse density is proportional to the specular density, a least squares fitting scheme for logarithms of mean transmissions was used to determine the proportionality constant for the instrumental set-up. The corresponding law relating specular to diffuse transmission values was then used to convert the measured transmission values in the Royal X wedge to those corresponding to a diffuse measurement, based on the Welch calibration.

The calibrated transmission values were then converted to opacity and density values for the purposes of determining a standard deviation measure for the noise. Mean values of opacity and density were, however, always calculated directly from mean calibrated transmission values. All processing of these data, once recorded on paper tape, was done in the 1604 computer.

The result of these measurements takes the form of a plot relating standard deviation values to mean values. Figure 5 shows such

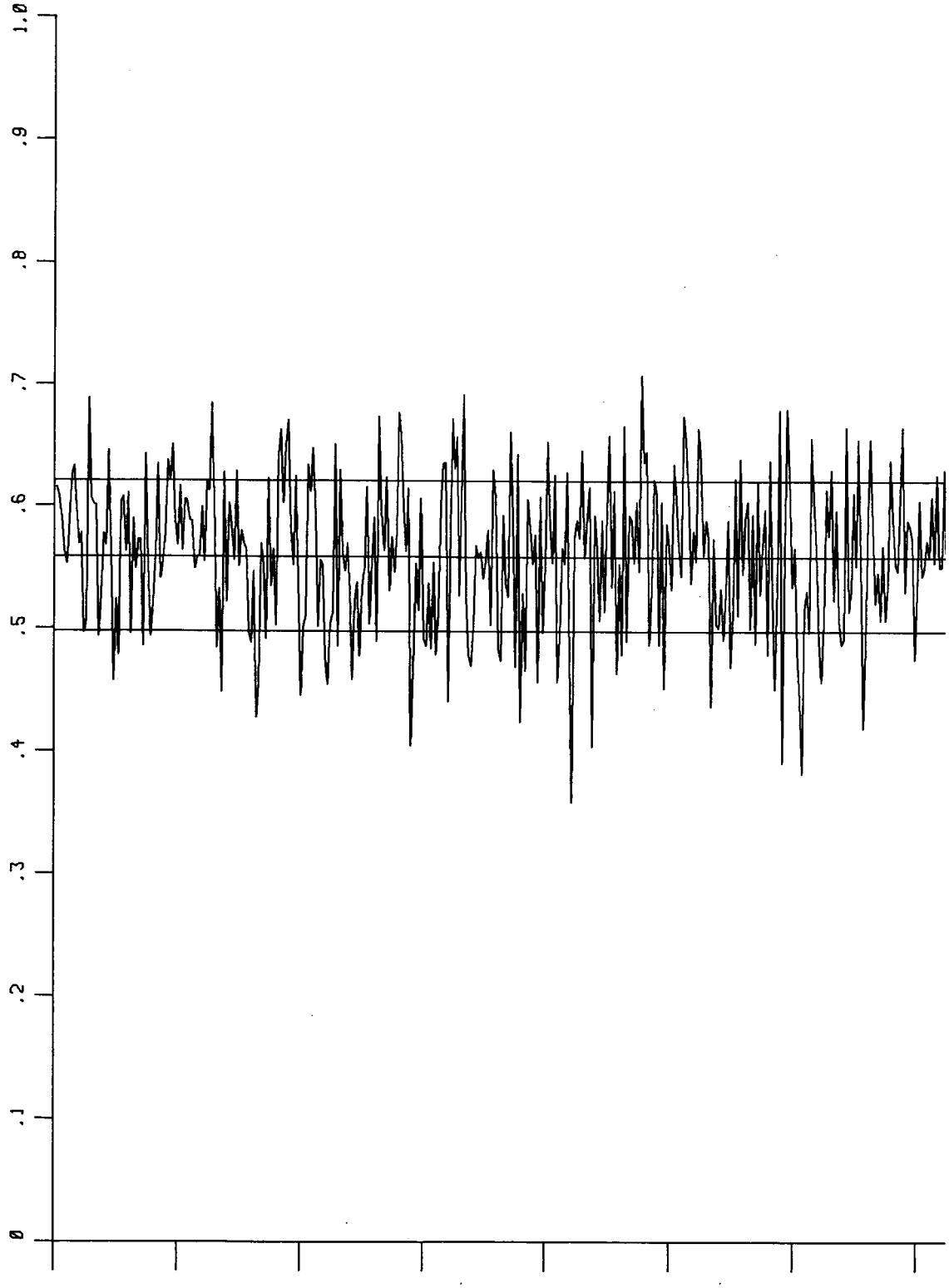

Fig. 4. Plot of paper tape record of transmission values measured from red-extended Royal-X Pan film.

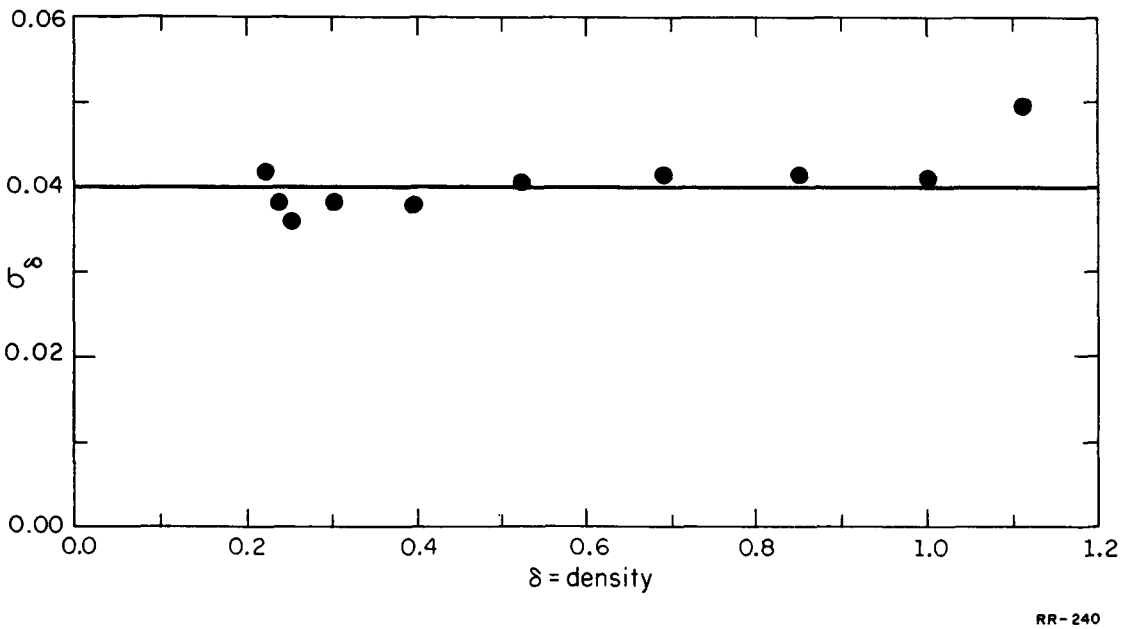

Fig. 5. Experimental values of standard deviation in density plotted vs. mean density.

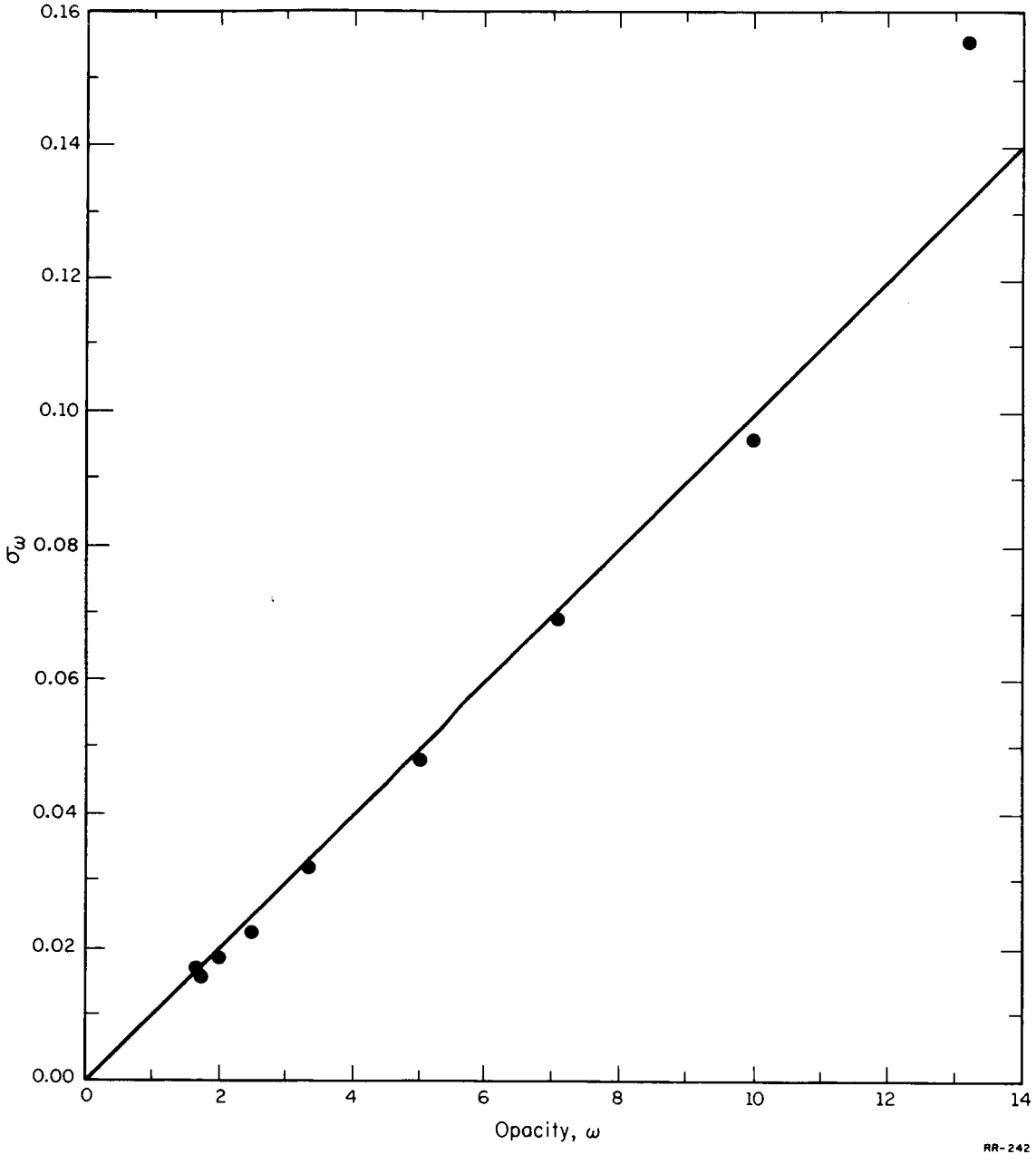

Fig. 6. Experimental values of standard deviation in opacity plotted vs. mean opacity.

a plot for density, and Fig. 6 shows such a plot for opacity. It is seen that the standard deviations in opacity σ_ω are consistent with a linear relation to the mean values ν_ω, and that this, in turn, is consistent with a constant standard deviation in density σ_δ. This observation is consistent with the expected differential relations. For example, suppose that σ_ω followed a power law:

$$\sigma_\omega = K\nu_\omega^\alpha \quad . \tag{10}$$

Then, since the density is

$$\delta = L\ln\omega$$

in which L = loge, and ln denotes natural logarithms, the differential density is

$$d\delta = \sigma_\delta = Ld\omega/\omega = L\sigma_\omega/\nu_\omega \ ,$$

so that one has

$$\sigma_\delta = LK\nu_\omega^{\alpha-1} \ , \tag{11}$$

provided that the standard deviations are small compared to the mean values. Thus if (10) describes a linear law ($\alpha = 1$), then (11) shows σ_δ to be independent of mean opacity and hence of mean density.

The $\alpha = 1$ interpretation appears to be valid for $1 < \nu_\omega < 10$ or $0 < \nu_\delta < 1$, a range of primary interest for the study of weak-exposure cases. In the months to come, more data is to be obtained for extending the range and for the purposes of consistency checks.

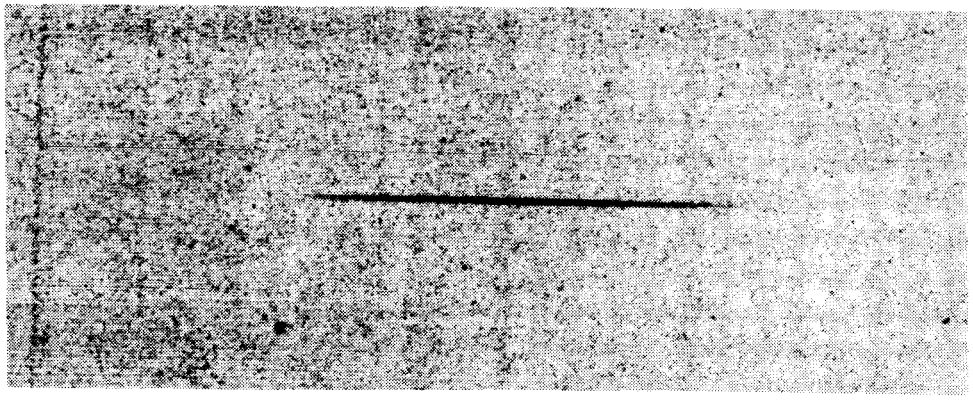

Fig. 7. Enlarged photograph of film image recorded by the anamorphic camera.

9. Analog Trials of Center Estimation

As described previously, an anamorphic optical system has been designed and constructed by which the sun's disc may be imaged as a long narrow ellipse, but with a resolution such that it will appear as a long streak of uniform width, but tapered illumination, exactly simulating the tapering of illumination within the unresolved flash pattern to be photographed in the relativity experiment. This image may be recorded to scale on 35 mm red-extended Royal-X Pan film. An enlargement of an early record of such an image is shown as Fig. 7. The original measures about 4400 μ in length corresponding to the 0.5 degree width of the sun's disc, for a 20 inch focal length. Densitometer tracings along the long axis of such an image resemble the plot of Fig. 3.

Center estimation trials are to be conducted on such images using the Jarrel-Ash Projection Microphotometer. A complete mock-up of an analog center estimator will not be undertaken, although an exploration of such instrumentation arrangements would be a part of a facilities development in preparation for the experiment. What is sought in this instance, however, is the most expedient means of obtaining analog confirmation of the computer simulation. For this reason, a dual-photocell double-wedge weighting scheme will not be used, and an admittedly more awkward double-pass procedure, using a single photocell with a single density wedge, will be followed.

The modifications required in the Jarrel-Ash machine are minimal for the use of the double-pass procedure, and may be designed so that the normal configuration may be speedily restored. It is this

fact that makes it possible to use the machine owned by the Astronomy Department during the hours when it is briefly available, and that makes it possible to proceed expediently and economically with this phase of the study. Most of the needed parts are at hand or may be readily fabricated, so that initial trials of the double-pass procedure are expected to be made shortly.

In the double-pass set-up, the photocell will be behind a slit oriented with its long axis along the long axis of the image. There will be a diffuser between the slit and the photocell so that the response of the photocell will be a nearly uniform function of the position of a light spot along the slit. This slit will be covered with a density wedge, and the response as a function of the position of a light spot along the slit will be measured to make a record of the weighting function being used. This will be done with the wedge in each of its two indexed orientations 180° apart. The records for these two positions together constitute the double-pass weighting function.

The procedure consists in translating the Mann stage in the direction of the long axis of the image until the image enters the slit at the latter's high-density end and moves along the slit to the position just short of emerging at the low-density end. At this point the position of the stage is recorded together with the transmission value. After the wedge is turned, the above pass is repeated stopping at a point judged not "by eye," this time, but at a point where the transmission value is the same as before. The average in positions is then taken as the center estimate.

The anamorphic camera produces a pair of such images with fixed relative positions on each frame. The datum for statistical analysis is the difference in center estimate, along their long axes, between these two images. These data will be tabulated for a number of trials, each at a given peak density level, and the statistical measures of mean and standard deviation will be calculated for comparison with the results of computer simulation.

REFERENCES

1. Progress Report for June, July and August, 1965, Coordinated Science Laboratory, University of Illinois, pp. 11-22.

2. Progress Report for December, 1965, January and February, 1966, Coordinated Science Laboratory, University of Illinois, pp. 1-14.

3. Myers, J. L., Jr., "The Effects of Nodal Regression of the Orbit on the Gravity Gradient Precession of a Gyroscopic Satellite," Report R-309, Coordinated Science Laboratory, University of Illinois, July, 1966.

4. Karr, G. R., "Aerodynamic Torque on a Spinning Spherical Satellite with Application to Measurement of Accommodation Coefficients," Report R-295, Coordinated Science Laboratory, University of Illinois, May, 1966.

5. Progress Report for September, October and November, 1965, Coordinated Science Laboratory, University of Illinois, pp. 1-8.

6. Hill, D. W., "Calculation of the Spin-Axis Orientation of the Telestar Satellite from Optical Data," Bell System Technical Journal, November, 1963, pp. 2943-2960.

7. Evans, William J., "Aerodynamic and Radiation Disturbance Torques on Satellites Having Complex Geometry," Torques and Attitude Sensing in Earth Satellites, Ed. S. Fred Singer, 1964.

8. Roberson, Robert E., "Radiation Pressure Torques from Spatial Variations in Surface Properties," Journal of Spacecraft and Rockets, Vol. 2, No. 4, July-Aug. 1965, p. 605.

9. Chen, T. C., J. Hsu and D. Skaperdas, "Passive Damping of the General Relativity Satellite Gyro," Coordinated Science Laboratory Report R-330, University of Illinois, November, 1966.

10. Chree, C., Cambridge Phil. Soc. Trans., Vol. 14, Part 3 (1889), p. 292.

11. Barthel, H. O., "Effects of Micrometeorite Cratering on the Direction of the Axis of Maximum Moment of Inertia," CSL Report R-274, Coordinated Science Laboratory, University of Illinois, February, 1966.

12. Progress Report for March-August, 1966, Coordinated Science Laboratory, pp. 111-122, October, 1966.